The International Journal of Advanced Manufacturing Technology (2024) 131:4035–4053
https://doi.org/10.1007/s00170-024-13099-5

ORIGINAL ARTICLE

Geometric error compensation method using the Laser R-test

Tung-Hsien Hsieh[1,2] · Wen-Yuh Jywe[3] · Jheng-Jhong Zeng[2] · Chia-Ming Hsu[3] · Yu-Wei Chang[3]

Received: 26 October 2023 / Accepted: 22 January 2024 / Published online: 22 February 2024

Abstract

Traditional methods for measuring geometric errors in machine tools, including interferometry and Double Ball Bar (DBB), are known to be expensive and time-intensive. Consequently, a non-contact calibration system called the "Laser R-test" has been developed. This innovative system is designed to measure both position-independent geometric errors (PIGEs) and position-dependent geometric errors (PDGEs) efficiently. Since its development in 2000, this tool has been instrumental in analyzing eccentricity errors, angular position errors, and simultaneous trajectory errors. Through extensive research, it has been determined that the total error in a five-axis machine tool can be controlled to below 40 μm after compensating for eccentricity parameters and angular position errors. However, reducing this error to below ± 10 μm is challenging, primarily due to wobble errors in the orientation of the rotary axis without compensating. In this study, a new methodology based on Laser R-test and Rodrigues' rotation formula has been developed to establish a PIGE model of rotary axis. Based on the methodology, the 8 PIGEs can be analyzed by measuring 5 coordinate positions. The compensation of 8 PIGEs in the rotary axis is completed within 30 min using the inspection path. Compatibility with ISO-10791–6 standards for BK1, BK2, and BK4 path tests is confirmed, validating the compensation effects. A precision of below ± 10 μm is achieved, with inspection time reduced by over 50%. This system can complete multiple errors by simply using the different paths. This greatly reduces the setup time for future users, enhancing its commercial applicability.

Keywords Error compensation · Rotary axis error · Optical measurement · Multi-axis simultaneous error · Concentricity error · Wobble error

Highlights

1. Enhanced Precision: Achieved enhanced precision, reducing errors to within ± 10um in ISO 10791–6 K1 K2 K4 paths.
2. Rapid Analysis and Compensation: Completed error analysis and compensation in 30 min, reducing inspection time by 50%.
3. Comprehensive Error Detection: Enabled multiple error detections using different paths, offering versatile solutions.
4. Commercial Applicability: Validated benefits and reduced setup time showcase high commercial applicability.
5. Optimization of Five-Axis Performance: by compensating across 8 parameters, the simultaneous motion accuracy can be significantly optimized, achieving reductions of up to 10um.

1 Introduction

With the evolution of the times and the advancement of technology, consumers and manufacturers have increasingly stringent requirements for the quality and precision of the products they produce; and for the machine tools that play the role of production and manufacturing, in response to product demand, from the past three axis machine, gradually developed into a higher-level multi-axis machine tool.

✉ Tung-Hsien Hsieh
andycloud@nfu.edu.tw; a58503147@yahoo.com.tw

Wen-Yuh Jywe
jywe29@ntu.edu.tw; jywe1219@gmail.com

Jheng-Jhong Zeng
zjjhong81@gmail.com

Chia-Ming Hsu
chia_ming1206@hotmail.com

Yu-Wei Chang
didi711x@yahoo.com.tw

[1] Department of Automation Engineering, National Formosa University, Yunlin, Taiwan

[2] Smart Machinery and Intelligent Manufacturing Research Center, National Formosa University, No.64, Wunhua Rd., Huwei Township, Yunlin County 632, Taiwan

[3] Department of Mechanical Engineering, National Taiwan University, No. 1, Sec. 4, Roosevelt Rd., Taipei 106319, Taiwan

Among the error sources of the machine tool, the static error is the main element that causes the difference in the accuracy of the machine tool. The geometric errors in the static error includes the component errors that produces different error amounts with the movement of the machine tool's assembly components, and the location errors that does not change as the assembled component moves. In the high-end five-axis machine tool structure, there are usually three linear axes that move linearly and two rotary axes that rotate axially. Due assembly and manufacturing errors, the geometric errors in machine tools are divided into position-independent geometric errors (PIGEs) and position-dependent geometric errors (PDGEs). In the three linear axes of a machine tool, there are 3 PIGEs, and each linear axis exhibits 6 PDGEs. Additionally, the two rotary axes together account for a total of 22 geometric errors, consisting of 10 PIGEs and12 PDGEs. Therefore, in a high-end five-axis machine tool, there are 43 geometric errors. ISO 230 and ISO 10791–6 in the specifications of the International Organization for Standardization (ISO) stipulate the accuracy standards for traditional three-axis machine tools and high-end five-axis machine tools.

The moving path is used as the basis for judging whether the precision of the advanced machine tool meets the standard. The precision adjustment method of the machine tool is mainly produced by assembly technology, allowable tolerance range, and structural design of the assembly personnel when each component is assembled. With the change of structural rigidity caused by the wear and tear of components for a long time, the accuracy of the machine tool can no longer be compared with the state of the new machine as just out of the factory. It is not economical to disassemble the components and reassemble them. Thus, the adjustment of the machine tool accuracy in the later stage is mainly completed by adjusting the parameters through the controller. To adjust the controller parameters, a calibrated detection device is required to obtain the error generated by the machine tool during the traveling process, and through the error to correct the machine tool's accuracy.

1.1 Research motivation and background

The five-axis machine tool consists of three linear axes (*X*, *Y*, and *Z* axes) and two rotary axes, which has exist 43 GE terms. Based on the structure of five-axis machine tools, the composition of the two rotary axes can be divided into two categories: either a combination of the *A*-axis and *C*-axis, a pairing of the *B* and *C* axes, or an arrangement of the *A*-axis and *B*-axis. The accuracy of the rotary axis is essential in a five-axis CNC machine tool, as it significantly influences the precision of five-axis machining operations. The two rotary axes have 22 GE items including the PDGEs and PIGEs [1–3].

The most general NC systems provide geometric error compensation functions, such as linear and angular position error compensation and thermal error compensation. Some advanced NC control systems even can provide PDGEs, PIGEs, and error volumetric compensation accessory, such as in HEIDENHAIN TNC640, Siemens 840D sl, and Fanuc 31i system.

Most of the machine tool accuracy detection equipment used at this stage is developed and sold by foreign manufacturers, such as RENISHAW, BLUM, and AGILENT. The related detection products are often expensive to purchase and maintain. Therefore, there is a certain threshold for domestic machine tool manufacturers to adjust the accuracy of their machine tools, and only some manufacturers with a certain scale can afford the abovementioned detection equipment costs.

Equipment companies such as RENISHAW CO. and H.P.Co. use an external high-precision rotating platform with a laser interferometer to detect the angle positioning error of the machine tool indexing table [4, 5], such as RENISHAW XR20-W and HP-E5290C and other products. IBS Precision Engineering developed the R-test system [6] to detect the total error of the five-axis machine tool. The IBS R-test system uses a capacitive probe. Due to the smaller sensing range of the capacitor, care must be taken during the system installation and setup process to avoid accidental collisions. Etalon developed a Laser TRACER high-speed automatic tracking laser length finder [7], which uses the GPS principle to automatically track the length data obtained by the laser to detect the three-dimensional error in the working space of the machine tool. In 2003, Tsutsumi [8] proposed a classical measuring method for PIGEs using conduct double ball bar (DBB) tests. The method has been accepted by many researchers and is included in ISO 10791–6 of test conditions for machining centers [9]. However, since the DBB is a one-dimensional sensor, multiple measurements are required to analyze a single error item, necessitating significant setup and measurement time. In 2011, Wen-Yuh Jywe and his team developed an optical non-contact detection system composed of four-quadrant sensors, lasers, and lens modules [10], based on the ISO-10791–6 testing method. This system can be used to detect errors in high-end and five-axis machine tools, such as eccentricity errors and five-axis motion trajectory errors(total error). This system can simultaneously detect errors in the *X*, *Y*, and *Z* directions. Therefore, it only needs to be set up once, and during a single measurement process, the *X*, *Y*, and *Z* trajectory errors during five-axis movement can be obtained simultaneously. This greatly reduces setup and measurement time, and the non-contact nature of the system minimizes the chance of collisions. Soichi Ibaraki's research introduces an enhanced non-contact R-test by using three laser triangulation displacement sensors[11]. This study focuses

on a new algorithm and laser sensor uncertainties to efficiently calibrate errors in five-axis machine tools, comparing its performance with traditional methods. As relevant scholars began to analyze the acquired measurement error trajectories, they often used mathematical methods to analyze PIGEs and PDGEs, aiming to improve the simultaneous five-axis trajectory errors and overall composite errors. Tran and Hsieh proposed a method for analyzing rotary axis angular positioning errors[12]. This method primarily uses the cosine theorem in a Cartesian system to address concentricity issues. Paired with the Laser R-test, it captures the optical scale *X*, *Y*, and *Z* coordinate signals of the linear axis. Through computation and analysis, the angular positioning errors of the *C*-axis or *A*-axis can be determined. Wang and his team [13] had introduced a method using a double ball bar (DBB) and unit dual quaternion (UDQ) to identify position independent geometric errors in five-axis machines. This approach had simultaneously pinpointed eight distinct errors, streamlining experimental processes and operations, and had promoted enhanced machining precision through regular calibrations. In 2019, Li [14] presented a cost-effective method for compensating volumetric positioning errors in five-axis machine tools. By distinguishing between linear and nonlinear errors and utilizing sag error compensation with table multiplication, the method enhanced machine accuracy, showing promise in manufacturing. Its efficacy was confirmed using the NAS and S-shape test pieces. Guo [15] proposed a method for geometric error terms model, which is established based on the multibody system theory and the method of homogeneous transformation. Based on the proposed method, the 30 PDGEs and 13 PIGEs can be measured and analyzed by using DBB and XL-80 laser interferometer. The geometric error compensation results based on test experiments of cutting impellers showed that the accuracy of the machined parts with complex curved surfaces was improved 56.22%. In 2023, Yao et al. [16] have developed an innovative method to simultaneously identify PDGEs and PIGEs in dual rotary axes. By employing a laser tracker and two retroreflectors, the method allows for precise determination of PDGEs and PIGEs with a single setup, thus enhancing measurement efficiency. An identification model, integrated with the Powell algorithm, streamlines the error decoupling process. However, the widespread application of this method is currently limited due to the high cost of laser trackers. Cheng et al. [17] present a new test for identifying geometric and thermal errors in five-axis machine tools. Utilizing a specially designed disc-shaped test piece with 12 rectangular grooves, the method employs a coordinate-measuring machine for error detection. This process successfully pinpoints four PIGEs.

Based on previous studies and literature, it has been observed that for the precision of a five-axis machine tool, 70% of its error originates from the rotational axis PIGEs and PDGEs [18]. Currently, certain controller parameters within PIGEs and PDGEs are available, allowing users to make adjustments and compensations, mainly focusing on angular positioning errors like ECC, EAA, and EBB, and wobble errors such as XOC, YOC, AOC, BOC, and so forth. The majority of current research primarily employs interferometers and DBB, conducting multiple experiments and samplings before being able to analyze the corresponding geometric errors. One significant limitation of methods based on previous studies is the prolonged setup time and the ability to measure only a single error vector at one time.

This paper introduces an approach utilizing the Laser R-test, aiming to develop a speedy detection path and technique to concurrently measure the five-axis machine tool's angular positioning error, eccentricity error, and wobble error of the rotational axis. The core of this research presents a 4×4 matrix coordinate analysis method, combined with the Rodrigues' rotation formula principle, to establish a wobble error model. Primarily, through the Laser R-test, the *X*, *Y*, and *Z* coordinate changes during the sensing movement path are measured. By incorporating these *X*, *Y*, and *Z* coordinate changes into the wobble error model, the corresponding PIGEs can be ascertained. This method promises a significant reduction in error measurement time and simplifies the complexity of model derivation. Lastly, this research will plan experiments to validate and compare the benefits of compensating for different PIGE parameter items concerning the trajectory errors of the five-axis machine tool. The measurement and compensation technique is adaptable for commercial CNC controllers, including HEIDENHAIN, SIEMENS, and FANUC.

2 A compensation method for five-axis machine tools

2.1 System configuration

This system, Laser R-test (LRT), was proposed in 2004 [10]. The original system hardware was for wired transmission and power supply. The current system has been developed to support Wi-Fi wireless transmission. The sampling frequency of the system is 1000 Hz, and it can be connected with the CNC controller. The LRT is an optical non-contact detection instrument independently researched and developed in Taiwan. The detection system includes two components as shown in Fig. 1: The first part is a 3D sensing module consisting of two sets of lasers and two quadrants of sensors. The second part includes a standard ball lens. Through the laser and photoelectric sensor modules combined with the optical glass imaging principle, the repeatability is about 1 μm, achieving

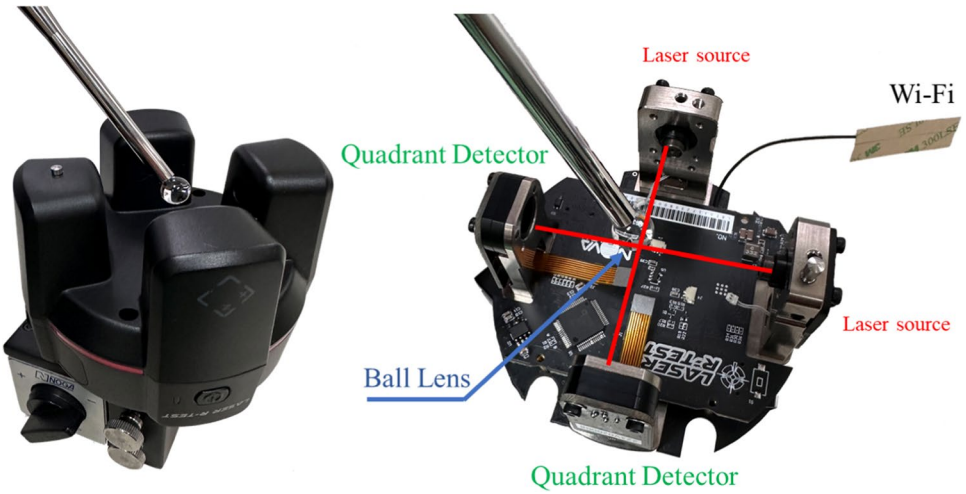

Fig. 1 The sketch of the Laser R-test key components

non-contact detection of machine tool error technology. LRT, the five-axis measurement system, has the following characteristics:

1. Biaxial sensing element can simultaneously obtain the machine tool space *X*, *Y*, and *Z* three-dimensional displacement signal. Compared with single-point contact measurement system, it can save measurement time.
2. Simple system architecture: users only need to set up the 3D sensing module and the optical ball lens seat on the machine tool spindle and the table end, respectively, and implement the precision detection path of the international standard ISO standard.

For the software interface, this research uses C# to develop an automatic compensation technology, and also through this research, an error analysis technology can be established. By the detection results of the ISO-10791–6 BK1 and BK2 path, the position errors of the spindle relative to the rotation axis can be analyzed, including any eccentric errors and yaw errors of the rotation axis. The human–machine interface is shown in Fig. 2.

2.2 System measurement method and principle

In this paper, the research focused on a five-axis machine tool with rotary axes *A* and *C* corresponding to the *X*, *Y*, and Z axes. Typically, five-axis machine tools exhibit

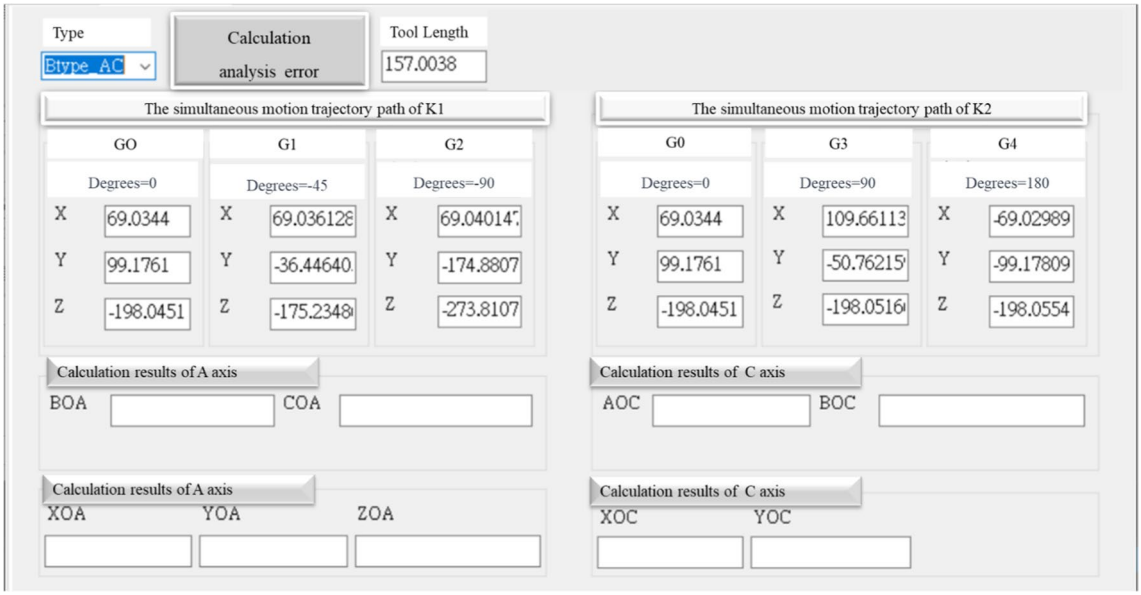

Fig. 2 The human machine interface of compensation method

eccentricity errors and gimbal errors. The eccentricity error can be calculated using a simple formula. Therefore, this study aimed to utilize the LRT system and spatial coordinate method to develop error models for AOC, BOC, COA, and BOA.

In general, two rotational axes of the five-axis machine tool often exhibit eccentricity errors and deflection errors. This study aims to utilize the LRT system and spatial coordinate methods to construct error models for AOC, BOC, COA, and BOA. The LRT system and spatial coordinate methods provide the necessary tools and techniques to accurately analyze and quantify the angular deflection errors in the rotational axes of the five-axis machine tool.

The rotation coordinate transformation matrices for a three-dimensional cartesian coordinate system based on the right-hand coordinate system [19] with X, Y, and Z axes, rotating by angles θA, θB, and θC, respectively. They are represented by Rx (θA), Ry (θB), and Rz (θC) as shown in (1),(2), and (3).

$$R_x(\theta_A) = \begin{bmatrix} 1 & 0 & 0 \\ 0 & \cos[\theta_A] & -sin[\theta_A] \\ 0 & sin[\theta_A] & \cos[\theta_A] \end{bmatrix} \tag{1}$$

$$R_y(\theta_B) = \begin{bmatrix} \cos[\theta_B] & 0 & sin[\theta_B] \\ 0 & 1 & 0 \\ -sin[\theta_B] & 0 & \cos[\theta_B] \end{bmatrix} \tag{2}$$

$$R_z(\theta_C) = \begin{bmatrix} \cos[\theta_C] & -sin[\theta_C] & 0 \\ sin[\theta_C] & \cos[\theta_C] & 0 \\ 0 & 0 & 1 \end{bmatrix} \tag{3}$$

Here, θA, θB, and θC represent the rotation angles around the X, Y, and Z axes, respectively. These matrices are used to describe the rotation transformations of an object in a three-dimensional cartesian coordinate system.

- The error model of AOC and BOC on the rotary table of C-axis

Placing the standard ball lens on the work table of the machine tool, the coordinates of point Pi (where $i = 1, 2, 3, \ldots, n$) are obtained. The X, Y, and Z values of the coordinates of the point can be simultaneously measured by the LRT. Based on this method, the standard ball lens is positioned on the C-axis table to obtain the coordinates of the first point $\mathrm{P1} = \begin{bmatrix} P1_x \\ P1_y \\ P1_z \end{bmatrix}$, and then, the C-axis is rotated to the angle θC to acquire the coordinates of the second point P2(c) without any AOC or BOC angle errors, As shown in Fig. 3, The matrix formula for P2(c) is given as shown in (4).

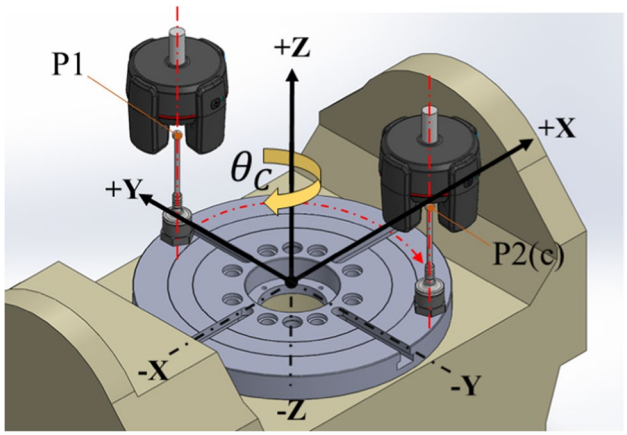

Fig. 3 The rotary table of C-axis, without AOC or BOC angle errors

$$\mathrm{P2}(c) = \begin{bmatrix} \mathrm{P2}(c)_x \\ \mathrm{P2}(c)_y \\ \mathrm{P2}(c)_z \end{bmatrix} = R_z(\theta_C) \bullet \begin{bmatrix} P1_x \\ P1_y \\ P1_z \end{bmatrix} \tag{4}$$

When the rotary table of C-axis has AOC and BOC angle errors, the coordinate transformation matrices for E_{AOC} and E_{BOC} are given by (5) and (6), respectively:

$$E_{AOC} = \begin{bmatrix} 1 & 0 & 0 \\ 0 & \cos[AOC] & -\sin[AOC] \\ 0 & \sin[AOC] & \cos[AOC] \end{bmatrix} \tag{5}$$

$$E_{BOC} = \begin{bmatrix} \cos[BOC] & 0 & \sin[BOC] \\ 0 & 1 & 0 \\ -\sin[BOC] & 0 & \cos[BOC] \end{bmatrix} \tag{6}$$

When the rotary table of C-axis has AOC and BOC angle errors, the matrix representation of the spatial coordinates can be expressed as (7):

$$E_{BOC} \cdot E_{AOC} = \begin{bmatrix} \cos[BOC] & sin[AOC]sin[BOC] & \cos[AOC]sin[BOC] \\ 0 & \cos[AOC] & -sin[AOC] \\ -sin[BOC] & \cos[BOC]sin[AOC] & \cos[AOC]\cos[BOC] \end{bmatrix} \tag{7}$$

When the rotary table of C-axis has AOC and BOC angle errors, the Z-axis vectors of rotary table of C-axis can be represented as (k_c).

$$\vec{(k_c)} = \begin{bmatrix} k_{Cx} \\ k_{Cy} \\ k_{Cz} \end{bmatrix} = \begin{bmatrix} \cos[AOC]sin[BOC] \\ -sin[AOC] \\ \cos[AOC]\cos[BOC] \end{bmatrix} \tag{8}$$

According to Rodrigues' formula method [20], in spatial coordinates, when rotating the Z-axis vector of a rotary table of C-axis with AOC and BOC errors by an angle θ_C, the formula for rotation can be expressed as follows, the spatial

coordinate representation $R_{\vec{k_c}}(\theta_C)$ can be calculated using the Rodrigues' formula as (9):

$$R_{\vec{k_c}}(\theta_C)=\begin{bmatrix} k_{Cx}k_{Cx}v\theta_C+c\theta_C & k_{Cx}k_{Cy}v\theta_C-k_{Cz}s\theta_C & k_{Cx}k_{Cz}v\theta_C+k_{Cy}s\theta_C \\ k_{Cx}k_{Cy}v\theta_C+k_{Cz}s\theta_C & k_{Cy}k_{Cy}v\theta_C+c\theta_C & k_{Cy}k_{Cz}v\theta_C-k_{Cx}s\theta_C \\ k_{Cx}k_{Cz}v\theta_C-k_{Cy}s\theta_C & k_{Cy}k_{Cz}v\theta_C+k_{Cx}s\theta_C & k_{Cz}k_{Cz}v\theta_C+c\theta_C \end{bmatrix} \tag{9}$$

$v\theta_C = 1-\cos\theta_C$, "$s$" represents the sine function (sin), and "c" represents the cosine function (cos).

As shown in Fig. 4, assuming P1 is located at any point on the rotary table of C-axis with AOC and BOC angle errors, and the Z-axis vector on the rotary table of C-axis is rotated by an angle θ_C to reach point $\mathrm{P2}(c)_\delta$, the calculation matrix for $\mathrm{P2}(c)_\delta$ is given by (10):

$$\mathrm{P2}(c)_\delta = R_{\vec{k_c}}(\theta_c)\cdot \mathrm{P1} \tag{10}$$

The spatial coordinates of $\mathrm{P2}(c)_\delta$ can be expressed as shown in (11).

$$\begin{bmatrix} \mathrm{P2}(c)_{\delta x} \\ \mathrm{P2}(c)_{\delta y} \\ \mathrm{P2}(c)_{\delta z} \end{bmatrix}=\begin{bmatrix} k_{cx}k_{cx}v\theta_c+c\theta_c & k_{cx}k_{cy}v\theta_c-k_{cz}s\theta_c & k_{cx}k_{cz}v\theta_c+k_{cy}s\theta_c \\ k_{cx}k_{cy}v\theta_c+k_{cz}s\theta_c & k_{cy}k_{cy}v\theta_c+c\theta_c & k_{cy}k_{cz}v\theta_c-k_{cx}s\theta_c \\ k_{cx}k_{cz}v\theta_c-k_{cy}s\theta_C & k_{cy}k_{cz}v\theta_c-k_{cx}s\theta_C & k_{cz}k_{cz}v\theta_c-c\theta_C \end{bmatrix} \tag{11}$$

To obtain the $\begin{bmatrix} \Delta X(c) \\ \Delta Y(c) \\ \Delta \mathrm{Z(c)} \end{bmatrix}$, $\Delta X(c)$, $\Delta Y(c)$, and $\Delta Z(c)$ error values caused by AOC and BOC errors of rotary table of C-axis, we can subtract the coordinates of point $\mathrm{P2}(c)_\delta$ (with AOC and BOC errors) from point *P2(c)* (without AOC and BOC errors). The resulting differences will represent the error values in each dimension, Mathematically, the error in the X-axis ($\Delta X(c)$), error in the Y-axis($\Delta Y(c)$), and error in the Z-axis ($\Delta Z(c)$) can be calculated as follows (12):

$$\begin{bmatrix} \Delta X(c) \\ \Delta Y(c) \\ \Delta \mathrm{Z(c)} \end{bmatrix}=\mathrm{P2}(c)_\delta - P2(c)=\begin{bmatrix} \mathrm{P2}(c)_{\delta x}-\mathrm{P2}(c)_x \\ \mathrm{P2}(c)_{\delta y}-\mathrm{P2}(c)_y \\ \mathrm{P2}(c)_{\delta z}-\mathrm{P2}(c)_z \end{bmatrix} \tag{12}$$

$\Delta X(c)$, $\Delta Y(c)$, and $\Delta Z(c)$ errors can be represented in spatial coordinates form as shown in (13).

$$\begin{bmatrix} \Delta X(C) \\ \Delta Y(C) \\ \Delta Z(C) \end{bmatrix}=\left(R_{\vec{k_c}}\begin{bmatrix} P1_x \\ P1_y \\ P1_Z \end{bmatrix}\right)-\left(R_Z(\theta_C)\bullet\begin{bmatrix} P1_x \\ P1_y \\ Pz \end{bmatrix}\right) \tag{13}$$

After expanding the matrix, we can obtain the calculation formulas for$\Delta X(c)$,$\Delta Y(c)$, and $\Delta Z(c)$ as follows:

$$\begin{aligned} \Delta X(C) =& -\mathrm{Cos}[\theta_C]P1_x+(\mathrm{Cos}[\theta_C]+\mathrm{Cos}[\mathrm{AOC}]^2 \\ & (1-\mathrm{Cos}[\theta_C])\mathrm{Sin}[\mathrm{BOC}]^2)P1_x-\mathrm{Sin}[\theta_C]P1_y \\ & +(-\mathrm{Cos}[\mathrm{AOC}](1-\mathrm{Cos}[\theta_C])\mathrm{Sin}[\mathrm{AOC}]\mathrm{Sin}[\mathrm{BOC}] \\ & +\mathrm{Cos}[\mathrm{AOC}]\mathrm{Cos}[\mathrm{BOC}]\mathrm{Sin}[\theta_C])P1_y \\ & +(\mathrm{Cos}[\mathrm{AOC}]^2\mathrm{Cos}[\mathrm{BOC}](1-\mathrm{Cos}[\theta_C])\mathrm{Sin}[\mathrm{BOC}] \\ & +\mathrm{Sin}[\mathrm{AOC}]\mathrm{Sin}[\theta_C])P1_z \end{aligned} \tag{14}$$

$$\begin{aligned} \Delta Y(C) =& \mathrm{Sin}[\theta_C]P1_x+(-\mathrm{Cos}[\mathrm{AOC}] \\ & (1-\mathrm{Cos}[\theta_C])\mathrm{Sin}[\mathrm{AOC}]\mathrm{Sin}[\mathrm{BOC}] \\ & -\mathrm{Cos}[\mathrm{AOC}]\mathrm{Cos}[\mathrm{BOC}]\mathrm{Sin}[\theta_C])P1_x \\ & -\mathrm{Cos}[\theta_C]P1_y+(\mathrm{Cos}[\theta_C]+(1-\mathrm{Cos}[\theta_C])\mathrm{Sin}[\mathrm{AOC}]^2)P1_y \\ & +(-\mathrm{Cos}[\mathrm{AOC}]\mathrm{Cos}[\mathrm{BOC}](1-\mathrm{Cos}[\theta_C])\mathrm{Sin}[\mathrm{AOC}] \\ & +\mathrm{Cos}[\mathrm{AOC}]\mathrm{Sin}[\mathrm{BOC}]\mathrm{Sin}[\theta_C])P1_z \end{aligned} \tag{15}$$

$$\begin{aligned} \Delta Z(C) =& (\mathrm{Cos}[\mathrm{AOC}]^2\mathrm{Cos}[\mathrm{BOC}](1-\mathrm{Cos}[\theta_C])\mathrm{Sin}[\mathrm{BOC}] \\ & -\mathrm{Sin}[\mathrm{AOC}]\mathrm{Sin}[\theta_C])P1_x+(-\mathrm{Cos}[\mathrm{AOC}]\mathrm{Cos}[\mathrm{BOC}] \\ & (1-\mathrm{Cos}[\theta_C])\mathrm{Sin}[\mathrm{AOC}]-\mathrm{Cos}[\mathrm{AOC}]\mathrm{Sin}[\mathrm{BOC}]\mathrm{Sin}[\theta_C])P1_y \\ & -P1_z+(\mathrm{Cos}[\mathrm{AOC}]^2\mathrm{Cos}[\mathrm{BOC}]^2(1-\mathrm{Cos}[\theta_C])+\mathrm{Cos}[\theta_C])P1_z \end{aligned} \tag{16}$$

By solving the simultaneous equations using (14), (15), and (16), the AOC and BOC errors can be obtained.

- The error model of BOA and COA on the rotary table of A-axis

As shown in Fig. 5, using the same principle, obtaining P2(A), θ_A is the rotation angle of the X-axis vector of the A-axis rotary table. Without any BOA or COA angle errors, point P1 is rotated by an angle θ_A to reach point

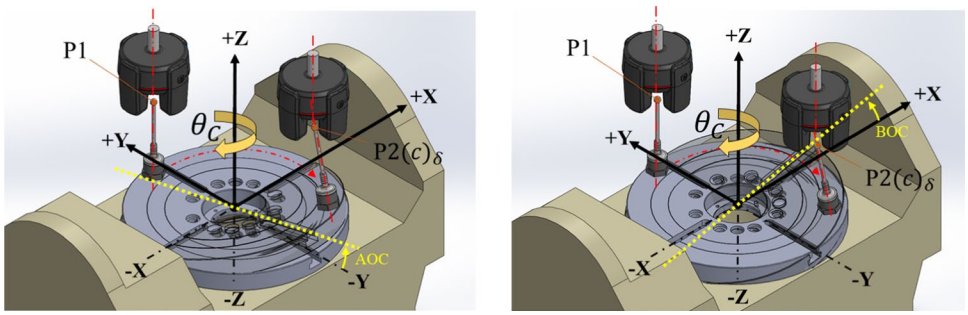

(A) AOC angular error (B) BOC angular error

Fig. 4 Diagram illustrating AOC and BOC angular errors in a rotary table of C-axis

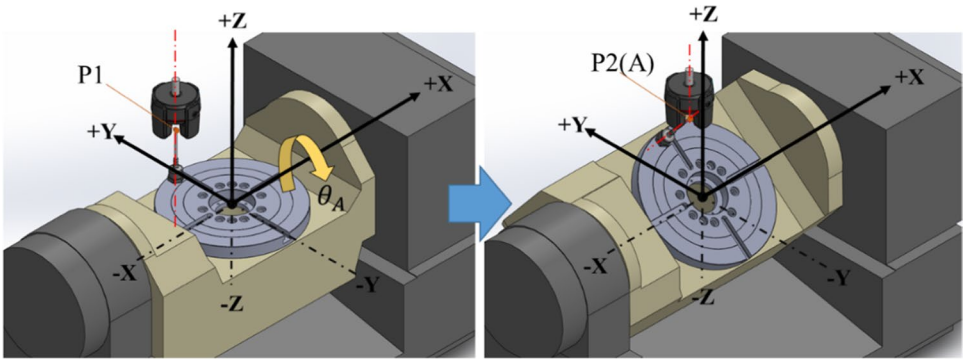

Fig. 5 The rotary table of A-axis with θ_A angle

P2(A). The matrix formula for P2(A) is given as shown in (17).

$$\begin{bmatrix} \mathrm{P2}(A)_x \\ \mathrm{P2}(A)_y \\ \mathrm{P2}(A)_z \end{bmatrix} = R_x(\theta_A) \cdot \begin{bmatrix} P1_x \\ P1_y \\ P1_z \end{bmatrix} \tag{17}$$

When the rotary table of A-axis has BOA and COA angle errors, the coordinate transformation matrices for E_{BOA} and E_{COA} are given by (18) and (19), respectively:

$$E_{BOA} = \begin{bmatrix} \cos[BOA] & 0 & sin[BOA] \\ 0 & 1 & 0 \\ -sin[BOA] & 0 & \cos[BOA] \end{bmatrix} \tag{18}$$

$$E_{COA} = \begin{bmatrix} \cos[COA] & -sin[COA] & 0 \\ sin[COA] & \cos[COA] & 0 \\ 0 & 0 & 1 \end{bmatrix} \tag{19}$$

When the rotary table of A-axis has BOA and COA angle errors, the matrix representation of the spatial coordinates can be expressed as (20)

$$E_{COA} \cdot E_{BOA} = \begin{bmatrix} \cos[BOA]\cos[COA] & -sin[COA] & cos[COA]sin[BOA] \\ \cos[BOA]sin[COA] & cos[COA] & sin[BOA]sin[COA] \\ -sin[BOA] & 0 & cos[BOA] \end{bmatrix} \tag{20}$$

When the rotary table of A-axis has BOA and COA angle errors, the X-axis vectors of rotary table of A-axis can be represented as (l_A).

$$\vec{(l_A)} = \begin{bmatrix} i_{Ax} \\ i_{Ay} \\ i_{Az} \end{bmatrix} = \begin{bmatrix} cos[BOA]cos[COA] \\ cos[BOA]sin[COA] \\ -sin[BOA] \end{bmatrix} \tag{21}$$

Based on the same principle, rewriting (9) allows the matrix $R_{\vec{l_A}}(\theta_A)$ can be obtain as shown in (22).

$$R_{\vec{l_A}}(\theta_A) = \begin{bmatrix} i_{Ax}i_{Ax}v\theta_A + c\theta_A & i_{Ax}i_{Ay}v\theta_A - i_{Az}s\theta_A & i_{Ax}i_{Az}v\theta_A + i_{Ay}s\theta_A \\ i_{Ax}i_{Ay}v\theta_A + i_{Az}s\theta_A & i_{Ay}i_{Ay}v\theta_A + c\theta_A & i_{Ay}i_{Az}v\theta_A - i_{Ax}s\theta_A \\ i_{Ax}i_{Az}v\theta_A - i_{Ay}s\theta_A & i_{Ay}i_{Az}v\theta_A + i_{Ax}s\theta_A & i_{Az}i_{Az}v\theta_A + c\theta_A \end{bmatrix} \tag{22}$$

As shown in Fig. 6, assuming P1 is located at any point on the rotary table of A-axis with BOA and COA angle errors, and the X-axis vector on the rotary table of A-axis is rotated by an angle θ_A to reach point $\mathrm{P2(A)}_\delta$, the calculation matrix for $\mathrm{P2(A)}_\delta$ is given by (23):

$$\mathrm{P2}(A)_\delta = R_{\vec{l_A}}(\theta_A) \cdot \mathrm{P1} \tag{23}$$

The spatial coordinates of $\mathrm{P2(A)}_\delta$ can be expressed as shown in (24).

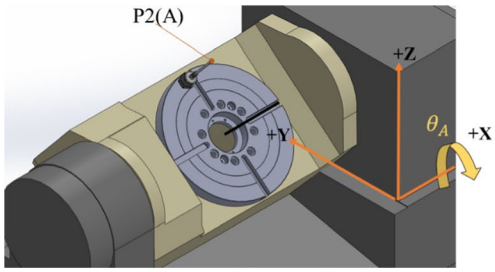

(A)Without BOA and COA angular error

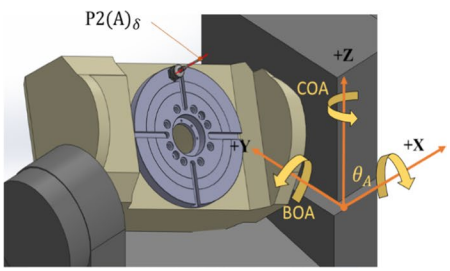

(B) with COA and BOAangular error

Fig. 6 Diagram illustrating BOA and COA angular errors in a rotary table of A-axis

$$\begin{bmatrix} \mathrm{P2(A)}_{\delta x} \\ \mathrm{P2(A)}_{\delta y} \\ \mathrm{P2(A)}_{\delta z} \end{bmatrix} = R_{\vec{l}_A}(\theta_A) \begin{bmatrix} P1_x \\ P1_y \\ P1_z \end{bmatrix} \tag{24}$$

Based on the same principle as (12) and (13), the error values for ΔX(A), ΔY(A), and ΔZ(A) can be obtained by (25).

$$\begin{bmatrix} \Delta\mathrm{X(A)} \\ \Delta\mathrm{Y(A)} \\ \Delta\mathrm{Z(A)} \end{bmatrix} = \mathrm{P2}_{\mathrm{A}\delta} - \mathrm{P2}_{\mathrm{A}} = \begin{bmatrix} \mathrm{P2(A)}_{\delta\mathrm{x}} - \mathrm{P2(A)}_{\mathrm{x}} \\ \mathrm{P2(A)}_{\delta\mathrm{y}} - \mathrm{P2(A)}_{\mathrm{y}} \\ \mathrm{P2(A)}_{\delta\mathrm{z}} - \mathrm{P2(A)}_{\mathrm{z}} \end{bmatrix} \tag{25}$$

The ΔX(A), ΔY(A), and ΔZ(A) errors can be obtained by calculation formulas as follows after expanding the matrix.

$$\begin{aligned} \Delta\mathrm{X(A)} = & -P1_x + (Cos[BOA]^2 Cos[COA]^2(1 - Cos[\theta_A]) + Cos[\theta_A])P1_x \\ & + (Cos[BOA]^2 Cos[COA](1 - Cos[\theta_A])Sin[COA] \\ & - Sin[BOA]Sin[\theta_A])P1_y + (-Cos[BOA]Cos[COA] \\ & (1 - Cos[\theta_A])Sin[BOA] - Cos[BOA]Sin[COA]Sin[\theta_A])P1_z \end{aligned} \tag{26}$$

$$\begin{aligned} \Delta Y(A) = & (Cos[BOA]^2 Cos[COA](1 - Cos[\theta_A])Sin[COA] \\ & + Sin[BOA]Sin[\theta_A])P1_x - Cos[\theta_A]P1_y + (Cos[\theta_A] \\ & + Cos[BOA]^2(1 - Cos[\theta_A])Sin[COA]^2)P1_y - Sin[\theta_A]P1_z \\ & + (-Cos[BOA](1 - Cos[\theta_A])Sin[BOA]Sin[COA] \\ & + Cos[BOA]Cos[COA]Sin[\theta_A])P1_z \end{aligned} \tag{27}$$

$$\begin{aligned} \Delta Z(A) = & (-Cos[BOA]Cos[COA](1 - Cos[\theta_A])Sin[BOA] \\ & + Cos[BOA]Sin[COA]Sin[\theta_A])P1_x + Sin[\theta_A]P1_y \\ & + (-Cos[BOA](1 - Cos[\theta_A])Sin[BOA]Sin[COA] \\ & - Cos[BOA]Cos[COA]Sin[\theta_A])P1_y - Cos[\theta_A]P1_z \\ & + (Cos[\theta_A] + (1 - Cos[\theta_A])Sin[BOA]^2)P1_z \end{aligned} \tag{28}$$

The BOA and COA errors can be obtained by solving the simultaneous equations represented by (26), (27), and (28). The definitions and explanations for the relevant symbols can be found in list of Method Symbols.

Table 1 The setting simulation parameters of errors

	PIGEs	Value
Wobble errors	AOC	0.001 ~ 0.005°
	BOC	0.001 ~ 0.005°
	COA	0.001 ~ 0.005° and 0.01 ~ 0.05°
	BOA	0.001 ~ 0.005° and 0.01 ~ 0.05°
Eccentricity errors	YOA	0 mm
	ZOA	− 500 mm
	XOC	0 mm
	YOC	0 mm

3 Error simulation and analysis

In this study, the initial setting parameters are presented in Table 1. The setup mechanical coordinates (distance from the center of the glass ball sphere to the reference point of the spindle) are $X = 0$ mm, $Y = 100$ mm, and $Z = -300$ mm. The tool length is 0 mm, and the eccentricity errors are XOC = 0 mm, YOC = 0 mm, YOA = 0 mm, and ZOA = − 500 mm. Subsequently, the *X*, *Y*, and *Z* directional errors for BK1 and BK2 can be simulated by incorporating AOC, BOC, COA, and BOA wobble errors into the formula using a passive approach.

It can simulate various errors' influence on the coordinate position of the spindle's nose point under synchronous measuring paths of any two linear axis BK1 and BK2 and a rotary axis. Taking the BK2 path as an example, when there is no error in BK2, the error of the tool nose point's position coordinates in the *X*, *Y*, *Z* direction is 0. When there is a yaw angle position error between the spindle and the rotation axis *C*, the *X*, *Y*, and *Z* directions of the AOC will be affected. When AOC = 0.001 degrees, there is ± 18 μm error in *X* direction, − 35 μm error in *Y* direction, and − 18 μm error in *Z* direction. Figure 7 is the error analysis graph while simulating AOC = 0.001 ~ 0.005°. When there is BOC = 0.001°, there is a 35 μm error in the *X* direction, ± 18 μm error in the *Y* direction, and ± 18 μm error in the *Z* direction. The following Figs. 7 and 8 are the error simulation results while simulating AOC and BOC = 0.001 ~ 0.005°. From the simulation results, it can be known that when there is a yaw angle error on the rotary axis, due to the Abbe principle, the error will be magnified and displayed on the coordinates of the final tool nose point, which means that it will cause the synchronous error to exceed the ISO standard. Thus, the same method can be used to simulate the influence of COA and BOA errors on the position coordinates of the tool nose point under the BK1 path. Figures 9 and 10 below show the error simulation results while simulating COA and BOA = 0.001 ~ 0.005° and 0.01 ~ 0.05°. Based on the simulation results, it is deduced that wobble errors in the *C*-axis or *A*-axis of a five-axis machine tool lead to errors in the *X*, *Y*, and *Z* directions, around 40 μm for the BK1 and BK2 paths. Thus, it becomes evident that compensating for these wobble errors in either the *A*-axis or *C*-axis is crucial for enhancing the overall accuracy of the five-axis machine tool.

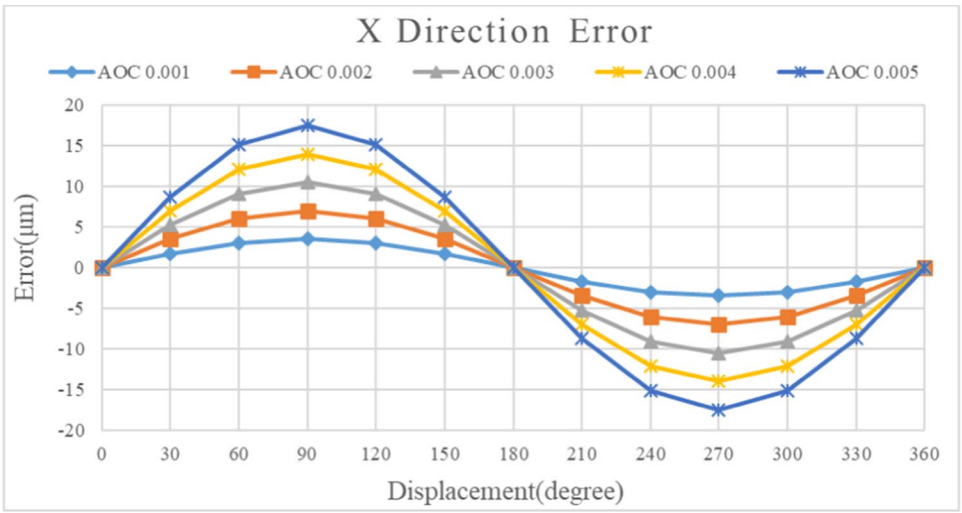

(A) X direction error

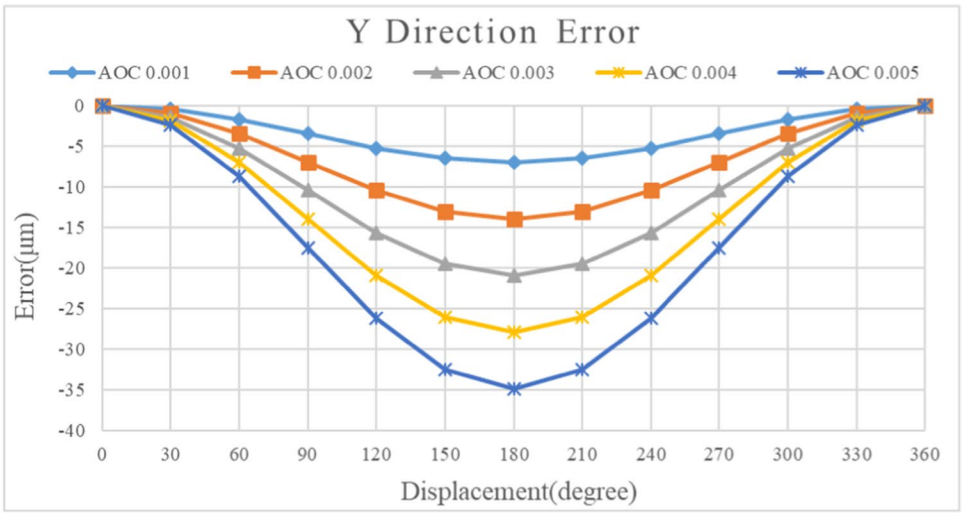

(B) Y direction error

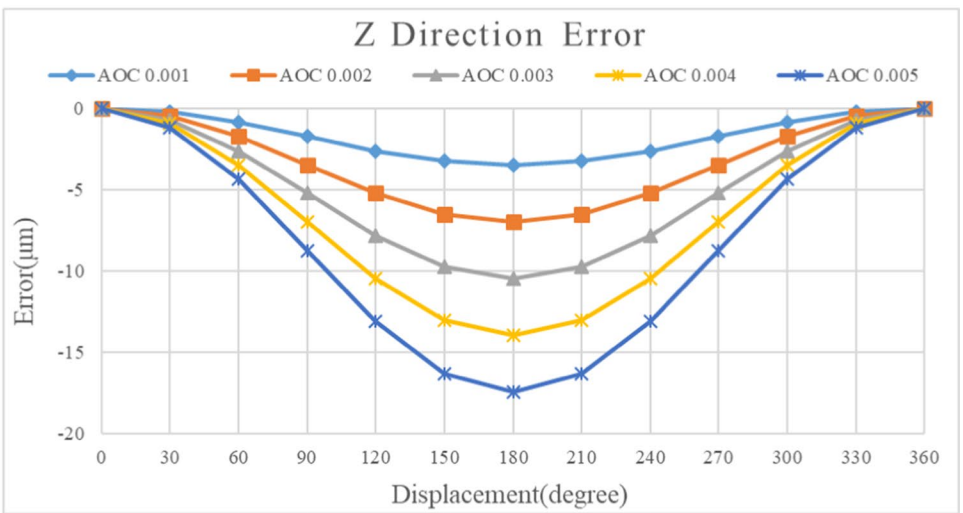

(C) Z direction error

Fig. 7 The BK2 simulation results with AOC error

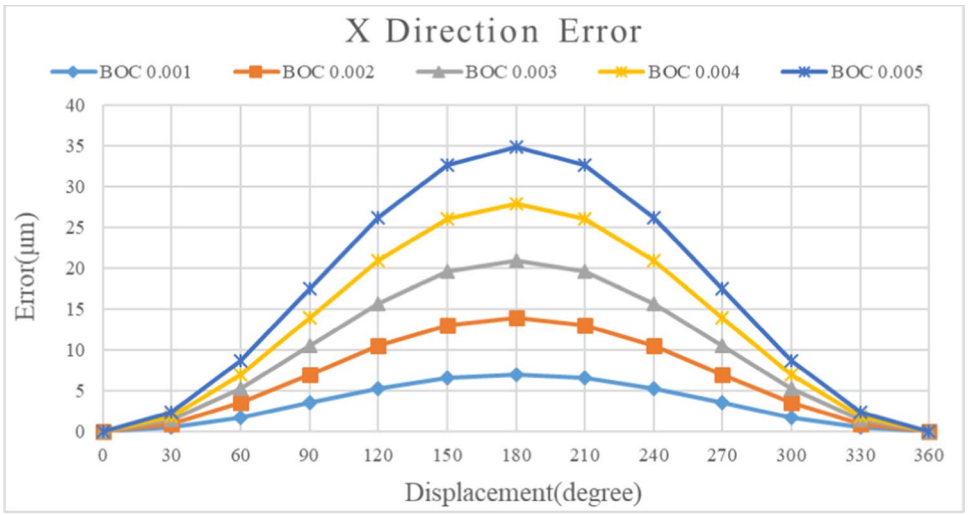

(A) X direction error

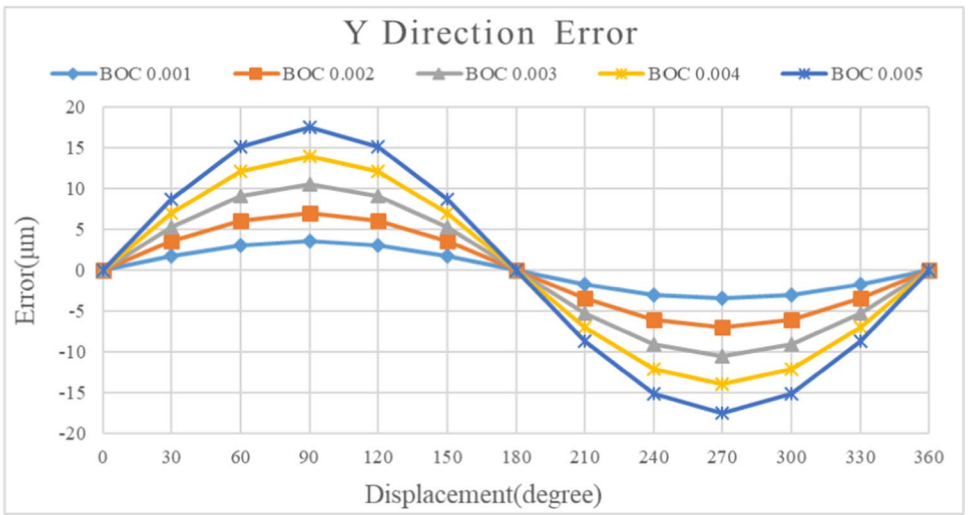

(B) Y direction error

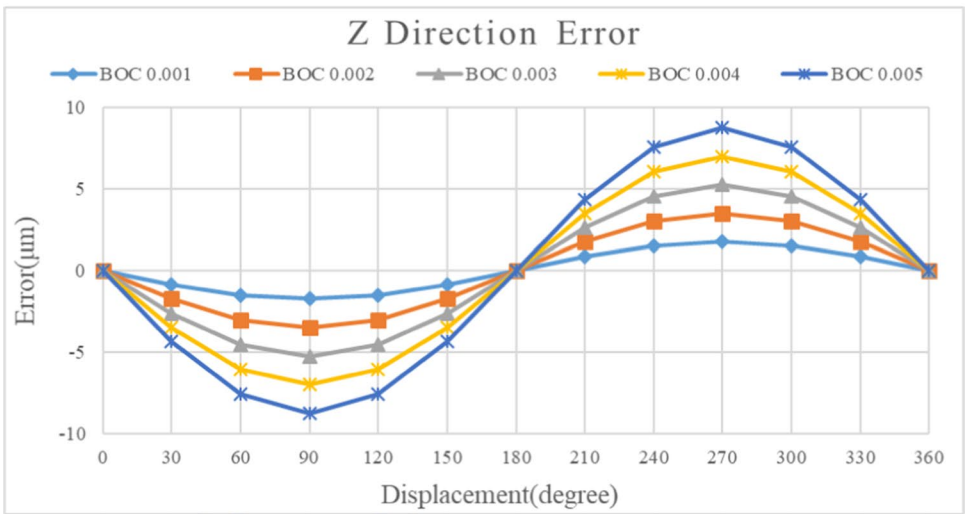

(C) Z direction error

Fig. 8 The BK2 simulation results with BOC error

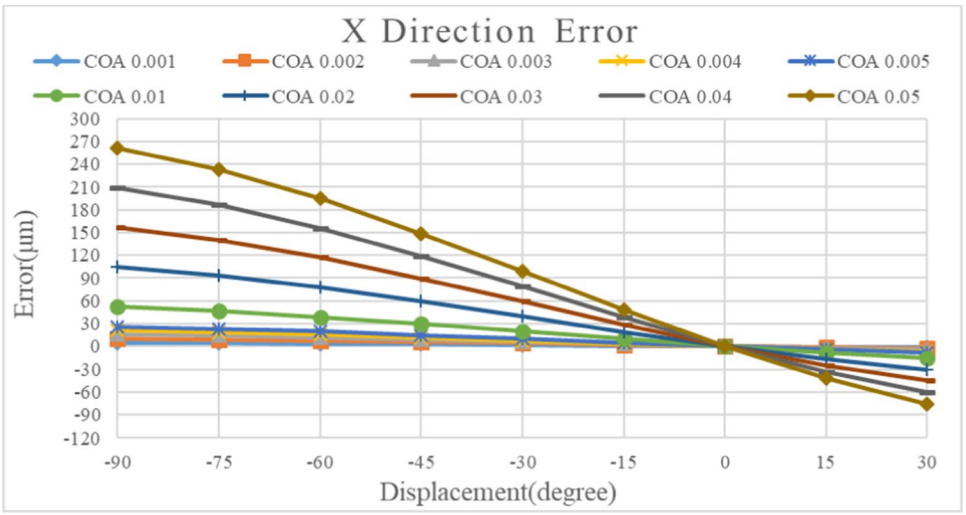

(A) X direction error

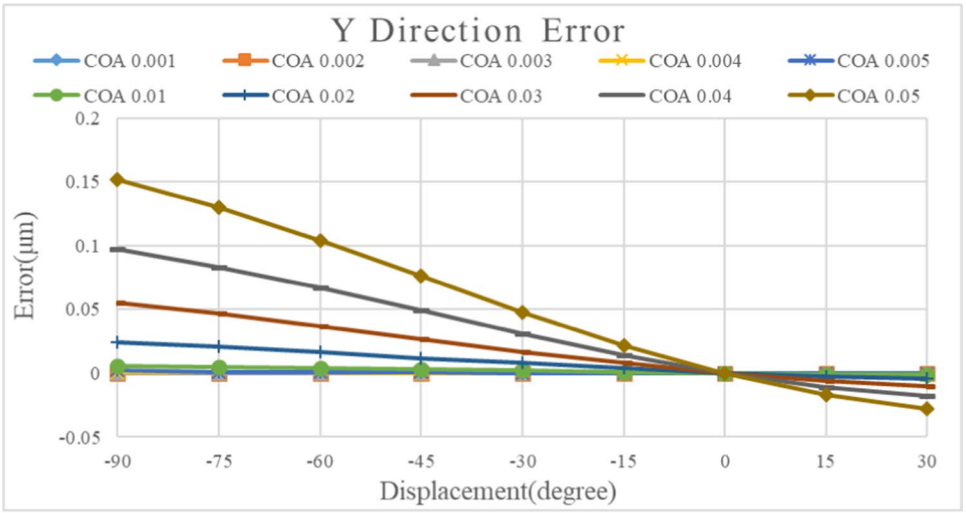

(B) Y direction error

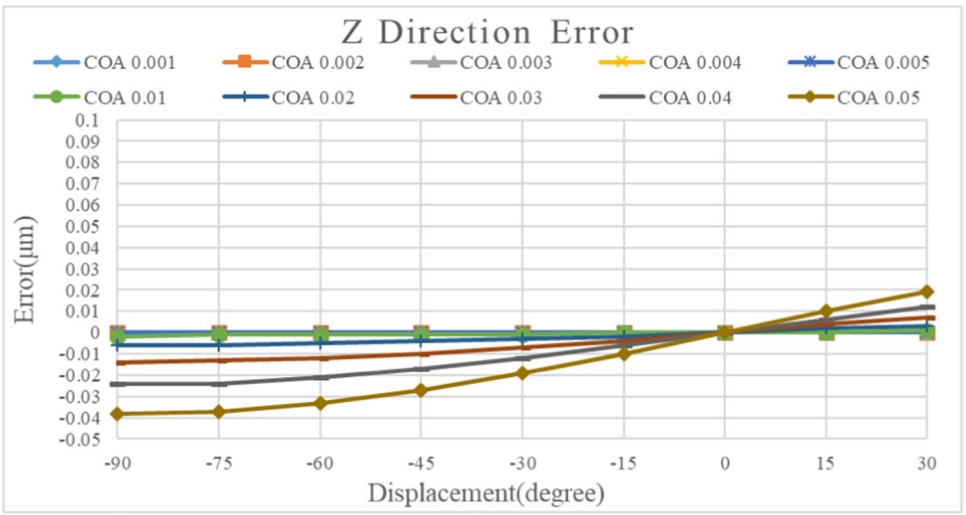

(C) Z direction error

Fig. 9 The BK1 simulation results with COA error

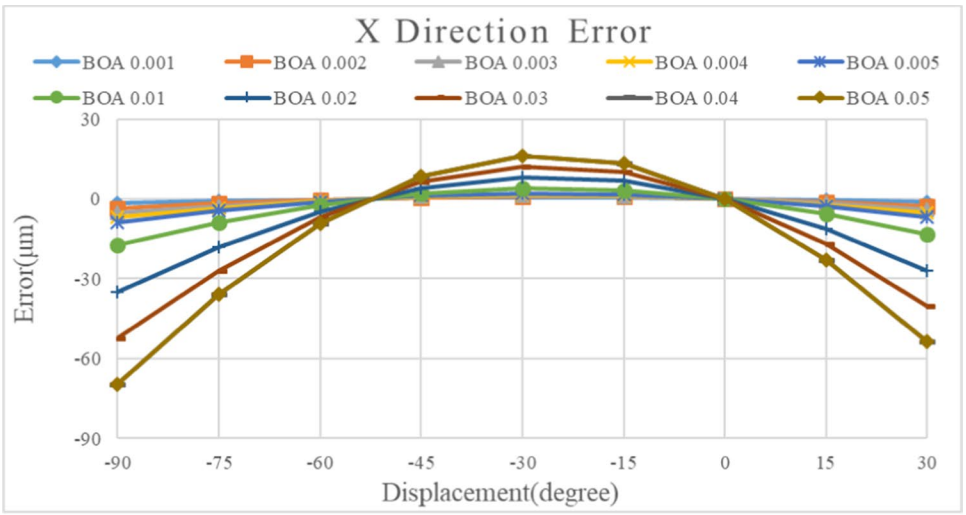

(A) X direction error

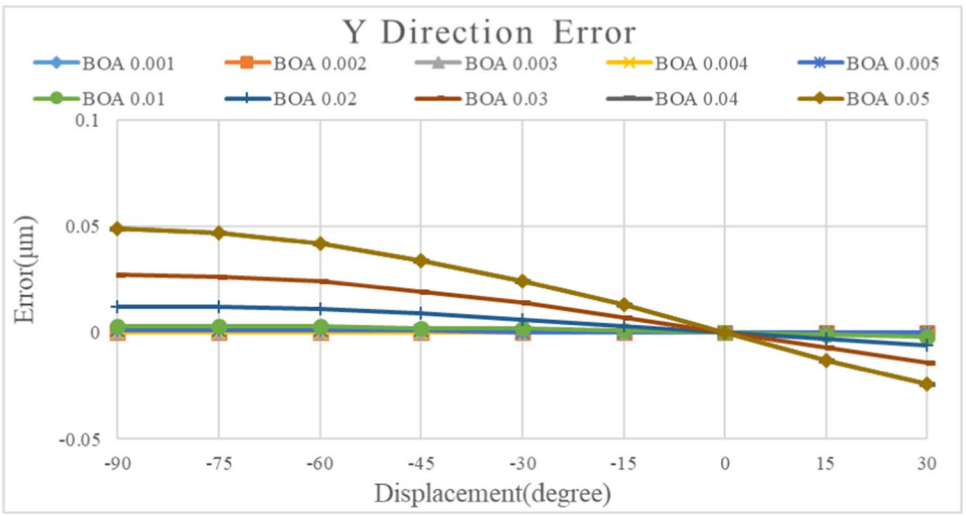

(B) Y direction error

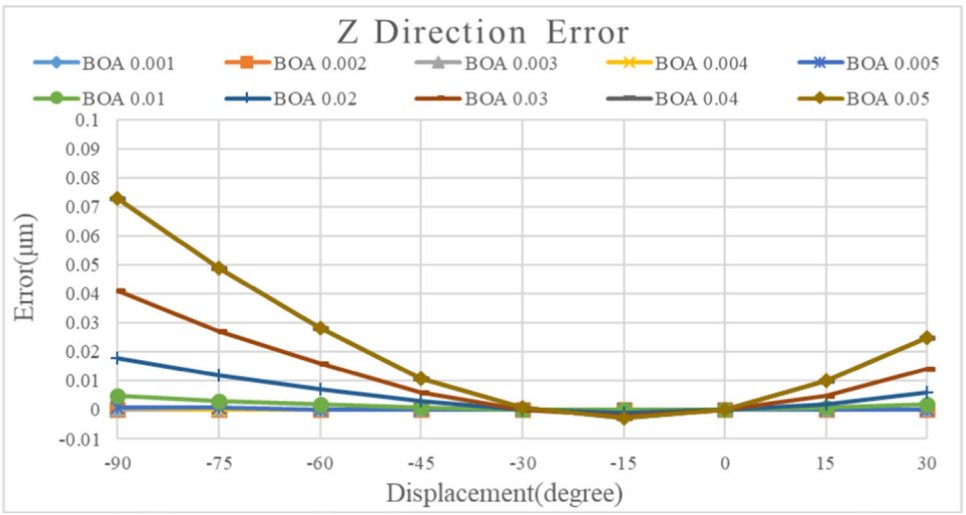

(C) Z direction error

Fig. 10 The BK1 simulation results with BOA error

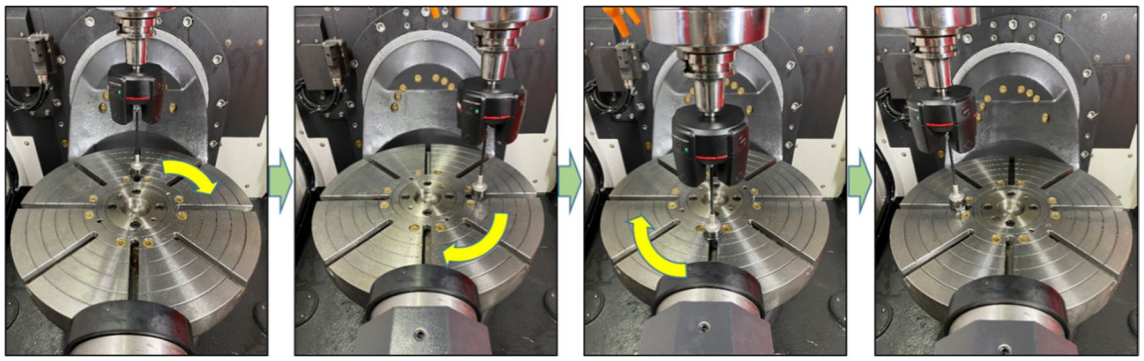

Fig. 11 Laser R-test system installation schematic diagram

Table 2 The coordinate positions based on under different trajectory paths

Sampled points	Coordinate positions of *X, Y*, and *Z*
G0	(0.311, 104.794, – 183.893)
G1	(104.772, – 0.289, – 183.8895)
G2	(– 0.311, – 104.751, – 183.8895)
G3	(– 104.1525, 104.791, – 284.729)
G4	(– 71.3045, 104.791, – 213.293)

Table 3 Analysis of 8 PIGEs based on different coordinate positions

PIGEs	Coordinate positions		
XOC	G0	G1	
YOC	G0	G1	
AOC	G0	G1	G2
BOC	G0	G1	G2
YOA	G0	G3	
ZOA	G0	G3	
BOA	G1	G3	G4
COA	G0	G3	G4

4 Experiment and results

The experimental method is to set up the LRT five-axis measurement system on the two ends of the five-axis machine tool spindle and the worktable. According to the international standard ISO 10791–6 machine tool accuracy detection path, the five-axis machine tool's multi-axis simultaneous motion path includes BK1 and BK2. Through the 3D sensing module, it can obtain the three-axis coordinate position under the machine tool simultaneous motion path, and calculate various errors during the motion of the five-axis machine tool rotating axis, including the rotation axis wobble error and rotation shaft eccentricity error.

The experiment planning is mainly divided into the following three steps. Step one is to perform data sampling and error analysis before uncompensated error parameters. Step two is to perform result verification and analysis after BC dual-axis eccentricity error compensation. Step three is to verify the results of BC rotation axis eccentricity and yaw error compensation and analysis. Laser R-Test System Installation Schematic, as shown in Fig. 11, involves the installation of an optical glass ball on the rotary axis platform. The 3D sensing module is mounted on the spindle. After rotating the rotary platform at different angles, sampling is performed sequentially to obtain the *X*, *Y*, and *Z* coordinate positions of the optical glass ball at each angle. Under different trajectory paths, the coordinate positions are sampled as follows (Table 2).

4.1 System sampling

In this study, coordinate positions on the under different trajectory paths sare sampled using a LRT. Coordinates such as G0, G1, G2, G3, and G4 are acquired, as illustrated in Table 2, with G0 typically designated as the initial coordinate position. These coordinates are then fed into the human–machine interface developed in this research, enabling the analysis of PIGEs for the *A*-axis or *C*-axis. The four PIGE parameters for the *C*-axis are derived by calculating the coordinates of G0, G1, and G2. Similarly, for the *A*-axis, its four PIGE parameters are ascertained by calculating the coordinates of G0, G3, and G4, as depicted in Table 3.

The first step: Using the *X*, *Y*, and *C* axes to move two points arbitrarily, and by using the LRT, it will obtain the coordinate positions of G0 and G1 points as

shown in the Table 2. The initial coordinate position of the system installation is represented by the G0 point. Inserting them into the formula and the human–machine interface (as shown in Fig. 2) developed in this research, the *C*-axis eccentric position parameter XOC YOC can be obtained.

The second step: Using the *X*, *Y*, and *C* axes to move three points arbitrarily, and by using the LRT, it will obtain the coordinate positions of G0, G1, and G2 points as shown in the Table 2 below by using the LRT. Inserting them into the formula and the human–machine interface developed in this research, the *C*-axis AOC and BOC errors can be obtained.

The third step: using the *Y*, *Z*, and *A* axes to move two points arbitrarily, and by using the LRT, it will obtain the coordinate positions of G0 and G3 points as shown in the Table 2. Inserting them into the formula and the human–machine interface developed in this research, the *A*-axis eccentric position parameters YOA and ZOA can be obtained. The fourth step: Using the *Y*, *Z*, and *A* axes to move three points arbitrarily, and by using the LRT, it will obtain the coordinate positions of G0, G3, and G4 points as shown in the Table 2. Inserting into the formula and the human–machine interface developed in this research, the *A*-axis BOA and COA errors can be obtained.

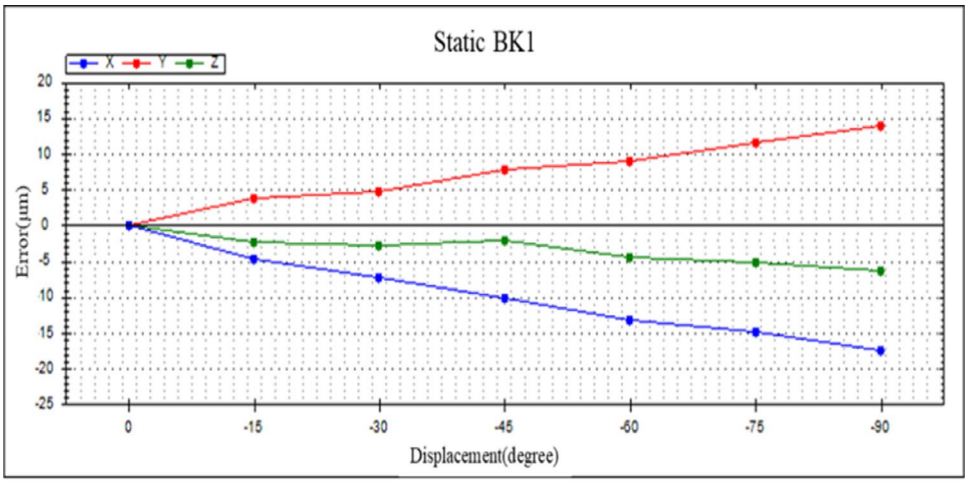

(A) BK1 trajectory path

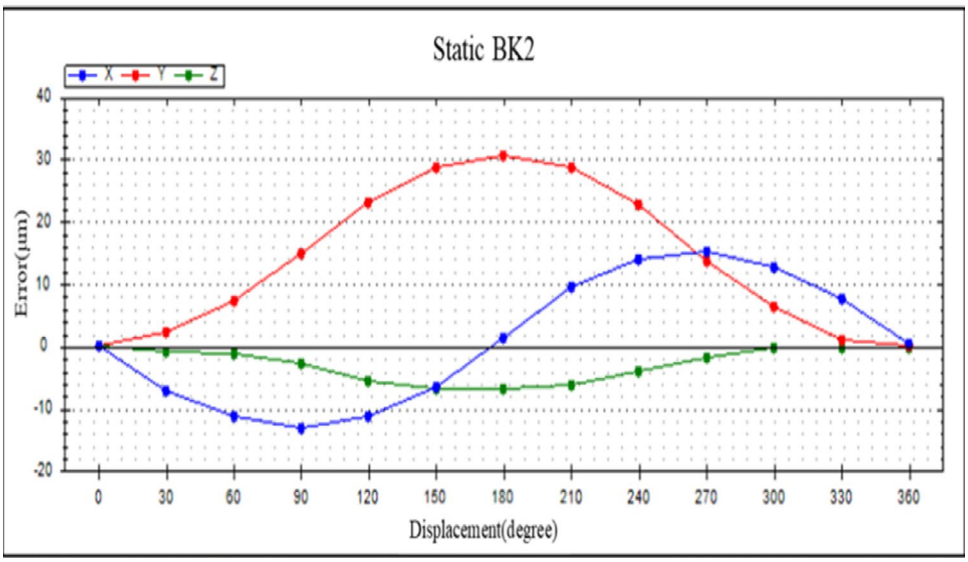

(B) BK2 trajectory path

Fig. 12 The results of BK1 and BK2 without compensating

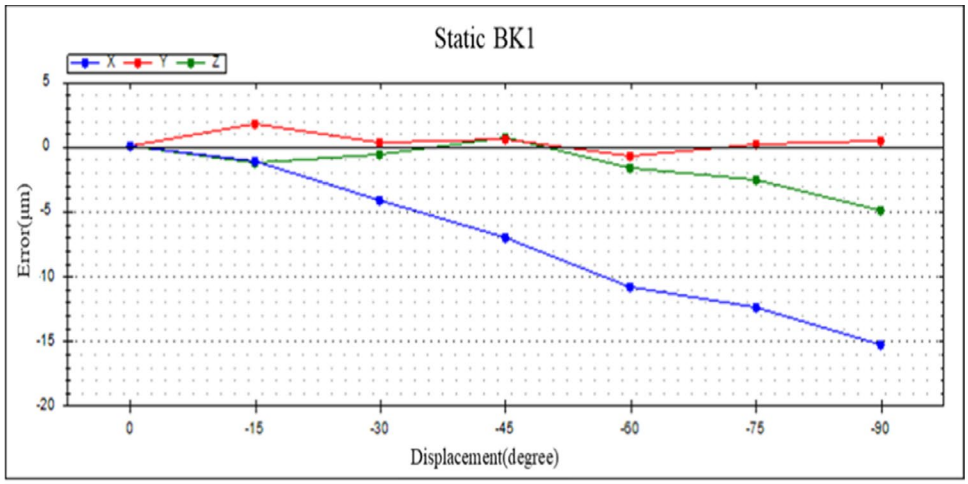

(A) BK1 trajectory path

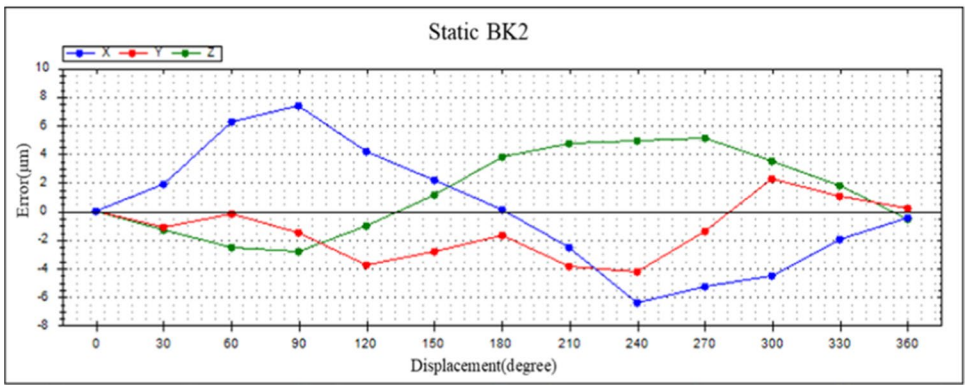

(B) BK2 trajectory path

Fig. 13 The results of BK1 and BK2 with compensating 4 parameters (modify eccentricity error)

4.2 Verification result and error analysis

Using ISO-10791–6 BK1:YZA synchronous motion and BK2:XYC synchronous motion path to compare eccentric error before and after compensation, it is found that from the result (as shown in Fig. 12) before BK2 compensation that there are sin and cos waves in the *X*-axis and *Y*-axis directions; the errors are 12 μm and 30 μm, respectively, and there is a jump error of about 8 μm in the *Z*-axis direction. After compensating for the eccentricity, the error of the *X*-axis and *Y*-axis can be significantly improved and reduced to 8 μm, but the direction error of the *Z*-axis still cannot be changed, so it can be understood that there may be a yaw error in the *C*-axis turntable.

Moreover, it is found that from the result (as shown in Fig. 13) before BK1 compensation, the direction error of the *X*-axis is particularly large. Therefore, after compensating the eccentric ZOA and YOA, the error compensation results can be effectively improved, and the errors in the *Y* and *Z* directions can be reduced to less than 5 μm, while the main wobble error of the rotating axis displayed in the *X* direction is approximately 16 μm of error, and cannot be eliminated or compensated.

The comparison between the results of the 4-parameter (XOC, YOC, ZOA, and YOA) compensation and the 8-parameter (XOC, YOC, ZOA, YOA, AOC, BOC, COA, and BOA) compensation will be performed using the BK1 and BK2 trajectory paths, employing the passive voice construction. It can be seen from Fig. 14A that the trajectory errors of the *X*, *Y*, and *Z* axes of BK1 can be reduced to within ± 5 μm. The errors caused by COA and BOA have been effectively reduced in the synchronous trajectory.

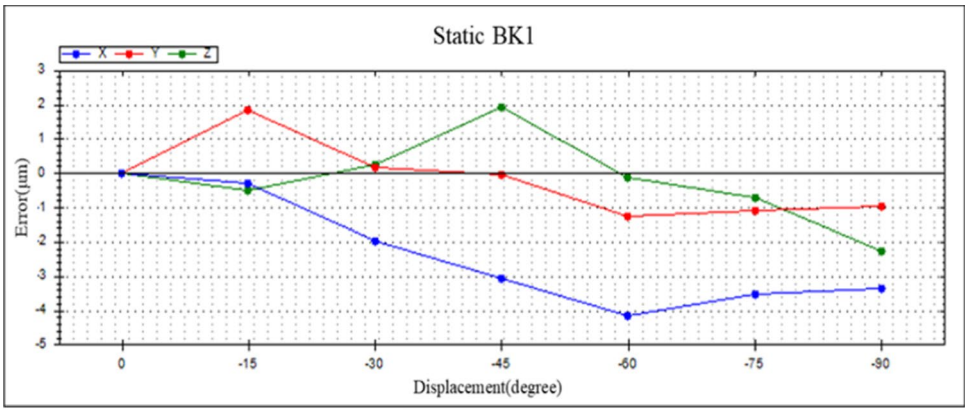

(A) BK1 trajectory path

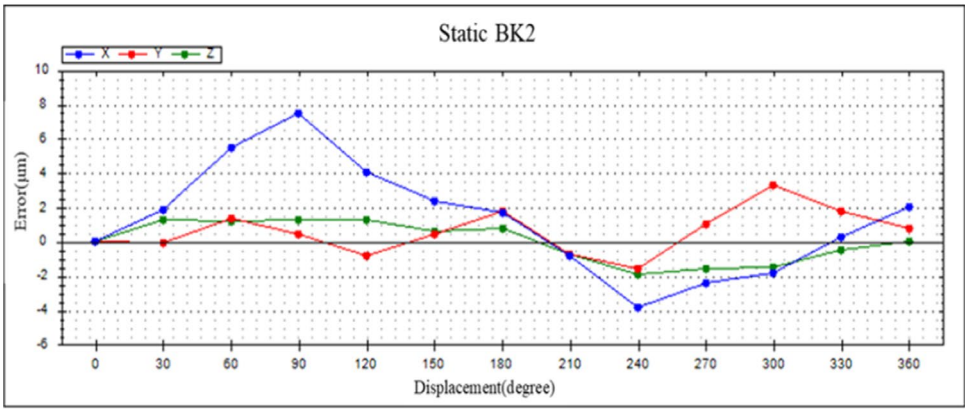

(B) BK2 trajectory path

Fig. 14 The results of BK1 and BK2 with compensating 8 parameters (modify eccentricity and wobble error)

Furthermore, from Fig. 14B, it can be observed that after compensation, the *Z*-direction trajectory error in BK2 has been reduced from the original 5 μm to within 2 μm. The significant influence of AOC and BOC on the synchronous trajectory error of BK2 has been effectively reduced.

Finaly, the ISO 10791–6 BK4 simultaneous motion path was utilized for verification, wherein the synchronous trajectory errors before and after compensating for the 4 and 8 parameters were compared. The results shown in Fig. 15 indicate that the errors in the five-axis synchronous trajectory have been reduced from approximately ± 80 μm to within ± 10 μm. Comparing the results of compensating for 4 parameters and 8 parameters, it was found that the error could be effectively reduced from ± 30 to ± 10 μm. The feasibility of the system and the derived method has been confirmed through the verification of the experimental results mentioned above. Through this method, the accuracy of multi-axis simultaneous motion has been effectively and significantly enhanced.

5 Conclusion and future works

The feasibility of the system hardware and analysis method has been verified, successfully analyzing 8 PIGE. Through the B-type structure and HEIDENHAIN controller TNC 640, this research validated the compensation benefits of different parameter items. Based on ISO-10791–6, the BK1, BK2, and BK4 paths completed the compensation test results under different compensation parameters. Finally, according to the compensation results, when only compensating for eccentricity errors such as XOC, YOC, ZOA, and YOZ, the BK1 and BK2 simultaneous motion errors are approximately ± 20 μm. After compensating for all 8 errors, the BK1 and BK2 simultaneous motion errors can be reduced to within ± 10 μm, and the BK4 five-axis simultaneous motion

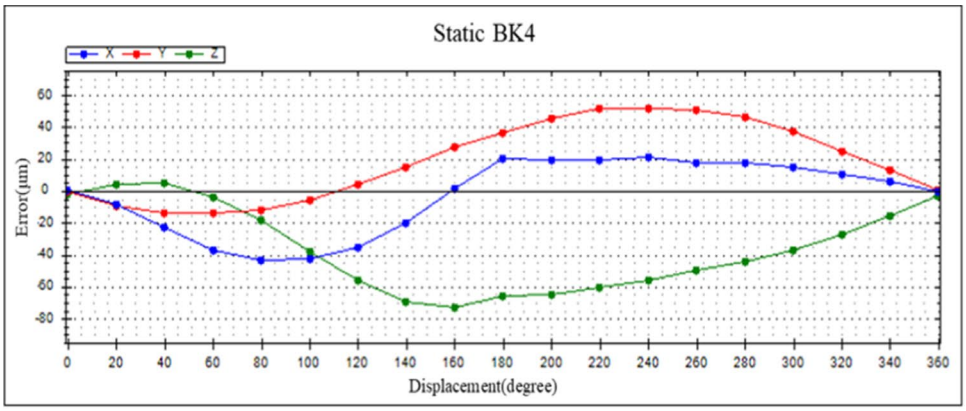

(A) before compensation

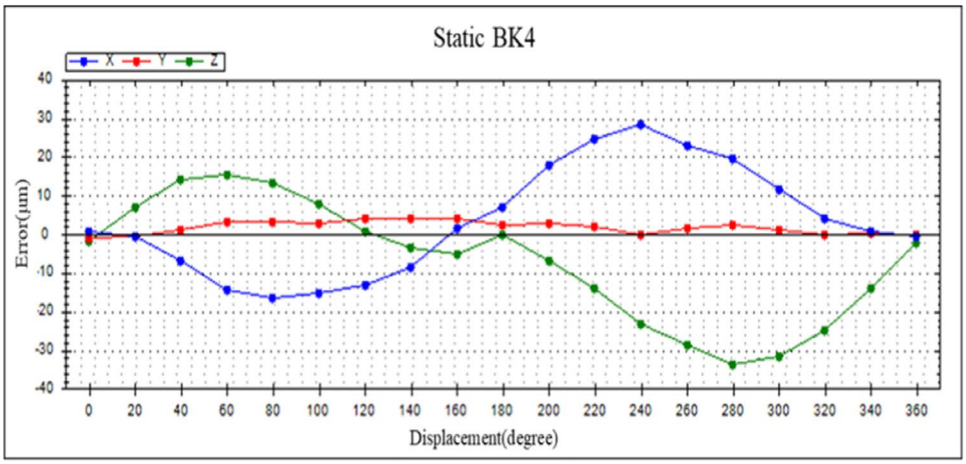

(B) after compensation with compensating 4 parameter

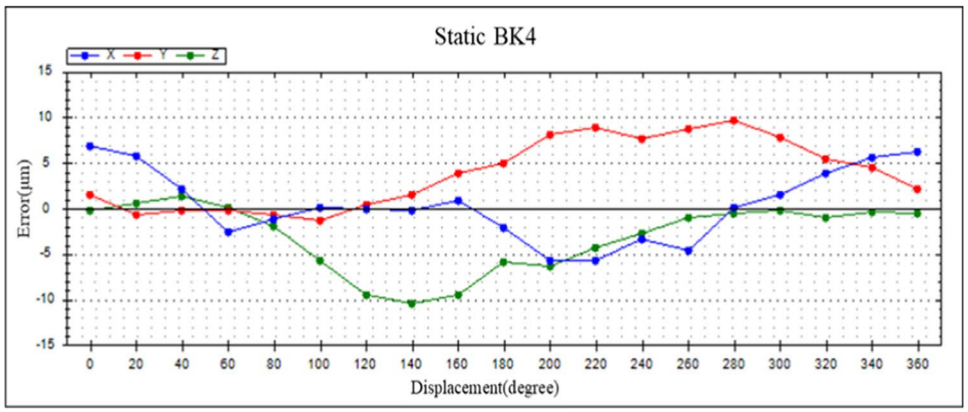

(C) after compensation with compensating 8 parameter

Fig. 15 The comparison results of BK4 trajectory error before and after compensation

errors can also be reduced to within ± 10 μm, significantly enhancing the precision of the five-axis machine tool. Moreover, with the same setup method, this system and method can complete multiple error detections, including angular positioning errors [12], eccentricity errors [10], and wobble errors, by simply using different paths. This greatly reduces the setup time for future users, enhancing its commercial applicability.

Symbols θA, θB, θC: The rotation angles around the X, Y, and Z axes, respectively; θ_x (θA): This is the rotation matrix for rotation about the X-axis by an angle θA; θy (θB): This is the rotation matrix for rotation about the Y-axis by an angle θB; θz (θC): This is the rotation matrix for rotation about the Z-axis by an angle θC; Pi (x, y, z): Pi represents a sampling point (where $i = 1, 2, 3, \ldots, n$, are not constant), with "i" being the sequential sampling order number, and the (x, y, z) denotes the coordinate position.; k_c : Z-Axis vectors of rotary table of C-axis; k_{Cx}, k_{Cy}, k_{Cz} : The Z-axis vector of the C-axis ration table is composed of the upper X, Y, and Z direction components; $R_{\vec{k}_c}$: The rotation matrix for the C-axis ration table around the Z-axis vector; E_{AOC}, E_{BOC}, E_{BOA}, E_{COA} : Coordinate transformation matrix for wobbles error (AOC, BOC, BOA, and COA); $P2(C)_{\delta(x,y,z)}$: When the C-axis is rotated with AOC and BOC errors, it results in obtaining the X, Y, and Z directional coordinate positions of $P2(C)_{\delta(x,y,z)}$.; $P2(C)_{(x,y,z)}$: When the C-axis is rotated without AOC and BOC errors, it results in obtaining the X, Y, and Z directional coordinate positions of $P2(C)_{(x,y,z)}$.; $\Delta X(C)$, $\Delta Y(C)$, $\Delta Z(C)$: Calculate the difference values in the X, Y, and Z directional coordinate between points $P2(C)_{\delta(x,y,z)}$ and $P2(C)_{(x,y,z)}$; l_A : X-Axis vectors of rotary table of A-axis; i_{Ax}, i_{Ay}, i_{Az} : The X-axis vector of the A-axis ration table is composed of the upper X, Y, and Z direction components; $R_{\vec{l}_A}$: The rotation matrix for the A-axis ration table around the X-axis vector; $P2(A)_{\delta(x,y,z)}$: When the A-axis is rotated without BOA and COA errors, it results in obtaining the X, Y, and Z directional coordinate positions of $P2(A)_{\delta(x,y,z)}$.; $P2(A)_{(x,y,z)}$: When the A-axis is rotated with AOC and BOC errors, it results in obtaining the X, Y, and Z directional coordinate positions of $P2(A)_{(x,y,z)}$.; $\Delta X(A)$, $\Delta Y(A)$, $\Delta Z(A)$: Calculate the difference values in the X, Y, and Z directional coordinate between points $P2(A)_{\delta(x,y,z)}$ and $P2(A)_{(x,y,z)}$

Acknowledgements I would like to express my gratitude to the Ministry of Science and Technology, Taiwan, for the integration program number MOST 110-2218-E-002-039, the Ministry of Economic Affairs, Taiwan for the program number MOEA 111AR02, and to cooperate with the manufacturers and National Formosa University for the industry-university cooperation to make this study go smoothly.

Author contribution This statement as follow reflects each author's significant role in the research process and publication of this paper. Tung-Hsien, Hsieh primarily contributed to the writing and revision of the manuscript, as well as planning the experimental methods. Wen-Yuh, Jywe mainly contributed to the conceptualization of the measurement system architecture, setting objectives, and planning and managing research activities. Jheng-Jhong, Zeng was primarily responsible for deriving and establishing the mathematical models. Chia-Ming, Hsu primarily contributed to the development and research of the measurement system hardware. Yu-Wei, Chang mainly contributed to conducting experimental tests, data collection, analysis, and compensation.

Declarations

Conflict of interest The authors declare the following financial interests/personal relationships which may be considered as potential competing interests: Tung Hsien Hsieh reports financial support and administrative support; article publishing charges, equipment, drugs, or supplies, and travel were provided by Ministry of Economic Affairs. Wen-Yuh Jywe reports financial support and administrative support; article publishing charges, equipment, drugs, or supplies, and travel were provided by Ministry of Science and Technology. Chia-Ming Hsu, Jheng-Jhong Zeng, and Yu-Wei Chang reports financial support and administrative support; article publishing charges, equipment, drugs, or supplies, and travel were provided by Ministry of Economic Affairs. Wen-Yuh Jywe, Chia-Ming Hsu, and Yu-Wei Chang reports a relationship with National Taiwan University that includes employment, non-financial support, and travel reimbursement. Wen-Yuh Jywe, Tung-Hsien Hsieh, Zhong-Liang Hsu, Chia-Ming Hsu, Yu-Wei Chang, Sen-Yi Huang, and Tung-Hsing Hsieh has patent Optical Detecting Apparatus for Detecting a Degree of Freedom Error of a Spindle and a Detecting Method Thereof issued to National Formosa University. Co-authors previously employed by National Formosa University: Yunlin Taiwan-Wen-Yuh Jywe, Chia-Ming Hsu, and Yu-Wei Chang.

References

1. Huang ND, Jin YQ, Bi QZ, Wang YH (2015) Integrated postprocessor for 5-axis machine tools with geometric errors compensation. Int J Mach Tools Manuf 94:65–73. https://doi.org/10.1016/j.ijmachtools.2015.04.005
2. Ibaraki S, Nagai Y (2017) Formulation of the influence of rotary axis geometric errors on five-axis on-machine optical scanning measurement-application to geometric error calibration by "chasethe-ball" test. Int J Adv Manuf Technol 92:4263–4273. https://doi.org/10.1007/s00170-017-0518-4
3. Abbaszadeh-Mir Y, Mayer JRR, Cloutier G, Fortin C (2002) Theory and simulation for the identification of the link geometric errors for a five-axis machine tool using a telescoping magnetic ball-bar. Int J Prod Res 40:4781–4797. https://doi.org/10.1080/00207540210164459
4. XR20-W Rotary Axis Calibrator. (n.d.). Retrieved September 30, 2023, from http://www.renishaw.com/en/xr20-w-rotary-axis-calibrator--15763
5. ISO 230–2(2014)- Part 2: determination of accuracy and repeatability of positioning of numerically controlled axes. Retrieved August, 2023, from https://www.iso.org/standard/55295.html
6. Bringmann B, Kung A (2005) A measuring artefact for true 3D machine testing and calibration. CIRP Anna 54(1):471–474. https://doi.org/10.1016/S0007-8506(07)60147-4
7. Etalonproducts.com. (2021). Etalon part of hexagon. Retrieved August, 2023. from http://www.etalonproducts.com/?option=com_content&task=view&id=48&Itemid=45&lang=en
8. Tsutsumi M, Saito A (2003) Identification and compensation of systematic deviations particular to 5-axis machining centers. Int J Mach Tools Manuf 43:771–780. https://doi.org/10.1016/S0890-6955(03)00053-1
9. ISO/DIS 10791–6 (2014) Test conditions for machining centers—part 6: accuracy of speeds and interpolations, Retrieved August, 2023, from https://www.iso.org/standard/46440.html
10. Jywe W, Hsu TH, Liu CH (2012) Non-bar, an optical calibration system for five-axis CNC machine tools. Int J Mach Tools Manuf 59:16–23. https://doi.org/10.1016/j.ijmachtools.2012.01.004
11. Hong C, Ibaraki S (2013) Non-contact R-test with laser displacement sensors for error calibration of five-axis machine tools. Precis Eng 37(1):159–171. https://doi.org/10.1016/j.precisioneng.2012.07.012

12. Tran CS, Hsieh TH, Jywe WY (2021) Laser R-test for angular positioning calibration and compensation of the five-axis machine tools. MDPI: Appl Sci 11(20):9507. https://doi.org/10.3390/app11209507
13. Wang, H, Jiang, X (2022) Geometric error identification of five-axis machine tools using dual quaternion. Int J Mech Sci, 107522. https://doi.org/10.1016/j.ijmecsci.2022.107522
14. Li, J, Mei, B, Shuai, C, Liu, XJ, Liu, D (2019) A volumetric positioning error compensation method for five-axis machine tools. Int J Adv Manuf Technol, pp.3979–3989. https://doi.org/10.1007/s00170-019-03745-8.
15. Guo, S, Mei, X, Jiang, G (2019) Geometric accuracy enhancement of five-axis machine tool based on error analysis. Int J Adv Manuf Technol, pp. 137–153. https://doi.org/10.1007/s00170-019-04030-4
16. Yao S, Huang H, Tian W, Gao W, Weng L, Zhang D (2023) Simultaneous identification for geometric error of dual rotary axes in five-axis machine tools. Meas 220:113368. https://doi.org/10.1016/j.measurement.2023.113368
17. Cheng T, Xiang S, Zhang H, Yang J (2023) New machining test for identifying geometric and thermal errors of rotary axes for five-axis machine tools. Meas 223:113748. https://doi.org/10.1016/j.measurement.2023.113748
18. Kvrgic VM, Ribic AI, Dimic Z, Zivanovic ST, Dodevska ZA (2022) Equivalent geometric errors of rotary axes and novel algorithm for geometric errors compensation in a nonorthogonal five-axis machine tool. CIRP J Manuf Sci Technol 37:477–488. https://doi.org/10.1016/j.cirpj.2022.03.001
19. Okafor AC, Ertekin YM (2000) Derivation of machine tool error models and error compensation procedure for three axes vertical machining center using rigid body kinematics. Int J Mach Tools Manuf 40:1199–1213. https://doi.org/10.1016/S0890-6955(99)00105-4
20. Kang Y-H, Huang B-H, Lu P-M, Xia Y (2017) Reverse engineering of a Hamiltonian for a three-level system via the Rodrigues' rotation formula. Laser Phys Lett 14(2):025201. https://doi.org/10.1088/1612-202X/aa512d
21. Florussen G, Houben K, Spaan-Burke T (2020) Automating accuracy evaluation of 5-axis machine tools. Int J Autom Technol 14(3):409–416. https://doi.org/10.20965/ijat.2020.p0409